ISSN 1024-8560, Atmospheric and Oceanic Optics, 2023, Vol. 36, No. 6, pp. 601–612. © Pleiades Publishing, Ltd., 2023.
Russian Text © The Author(s), 2023, published in Optika Atmosfery i Okeana.

SPECTROSCOPY OF AMBIENT MEDIUM

On the Uncertainty of the Calculated Intensities of Water Vapor Lines in the Sub-THz Frequency Range

R. I. Ovsyannikov[a], *, M. Yu. Tretyakov[a], **, M. A. Koshelev[a], *, and T. A. Galanina[a], ******

[a] *Gaponov-Grekhov Institute of Applied Physics, Russian Academy of Sciences, Nizhny Novgorod, 603950 Russia*

**e-mail: ovsyannikov@ipfran.ru*

***e-mail: trt@ipfran.ru*

****e-mail: koma@ipfran.ru*

*****e-mail: odintsova@ipfran.ru*

Received February 24, 2023; revised May 2, 2023; accepted May 3, 2023

Abstract—A comparative analysis of open source data on the water spectral lines intensities in the frequency range from 0 to 1.75 THz was carried out. The analyzed data are significant for radiation propagation models. The calculations by the method of effective Hamiltonians and the variational method, as well as experimental data were taken into account. The uncertainty of intensity was found to be less than 2% for lines of the ground vibrational state with an intensity of more than 10^{-27} cm/molecule and about 5–10% for weaker lines. For strong (more than 10^{-26} cm/molecule) rotational lines of the ν_2 state, the intensity uncertainty ranged from 2 to 5% and increased up to 5–10% for weak lines. For all rotational lines of the $2\nu_2$, ν_1, and ν_3 states, the uncertainty was no more than 5–10%. The presented data show that most of the considered lines can be assigned a higher (by 1–2 steps according to the classification adopted in HITRAN) category of intensity accuracy.

Keywords: line intensity, water molecule, subTHz, atmospheric absorption

DOI: 10.1134/S1024856023060131

INTRODUCTION

Information about the intensities of molecular spectral lines throughout the range from radio waves to ultraviolet is the basis for quantitative estimates of electromagnetic radiation absorption by the atmosphere. Such estimates are required in many spectroscopic applications associated with remote sensing of the atmosphere, for calculating the radiation budjet of the planet, a for modeling global climate changes. This work is highly topical as it will allow improving the accuracy of modeling one of the main components of atmospheric absorption, namely, the continuum associated with humidity, or non-resonant (non-selective) absorption of incoming solar and outgoing thermal radiation. The uncertainty of the continuum is currently one of the main factors limiting the accuracy of retrieving atmospheric parameters from remote sensing data both in the microwave [1] and in the near infrared ranges [2]. To date, the MT_CKD (Mlawer-Tobin_Clough-Kneizys-Davies) model [3, 4] is known as the only global semi-empirical model, which provides the continuum in the entire range of electromagnetic waves significant for the radiation balance from 0 to 20000 cm^{-1}. The model describes the observed continuum based on the modification of the wings of the resonant lines of water molecules at large frequency detuning from the center. The empirical coefficients of the model are regularly updated as new experimental data become available.

The main drawback of the model is that it does not take into account one of the most important physical mechanisms of continuum origin, namely, the dimerization of atmospheric gas molecules and the associated absorption of radiation by two interacting monomers (bimolecular absorption). On the basis of experimental data, it was proved [5–8] that due to this mechanism, characteristic dimer peaks appear in the spectrum of the continuum, which are responsible for a significant part of the observed continuum and can neither be predicted nor fully described within the framework of the MT_CKD model.

In view of lack of information for physically based modeling of the continuum (see, for example, [9] and references therein) the continuum is still determined empirically as the difference between the observed absorption and the calculated monomer H_2O spectrum. Therefore, the accuracy of determining the continuum depends on the accuracy of monomer spectrum calculation. Frequencies, intensities, the profile function, and the corresponding line parameters are needed for calculating the spectrum. Almost all the necessary information can be found in the HITRAN database [10]. However, our estimates [11] show that the uncertainty of the continuum component associ-

ated with the interaction of water molecules with dry air molecules (foreign continuum) in the region of the H_2O rotational band reaches 100% if the line parameters uncertainty codes from HITRAN are taken as the basis for calculations. Such a large uncertainty is caused by very cautious (up to an order of magnitude) error estimates in HITRAN, which makes it difficult to obtain reliable data on the continuum and to improve the accuracy of its modeling. To solve the problem, it is necessary to determine real error estimates of resonant line parameters.

The purpose of this work is to estimate the uncertainty of the water vapor line intensities in the frequency range up to 1.75 THz. Atmospheric absorption, including the continuum, in the spectral region up to 1 THz can be calculated using the MPM (Millimeter-Wave Propagation Model) [12–14], which is widely employed in remote sensing of the atmosphere using microwave radiometers (see, for example, [1] and references therein). We consider the 1–1.75 THz range so as to take into account their low-frequency wings (if the generally accepted cutoff of the wings at a detuning from the center of 25 cm^{-1} is used [15]), which can affect the spectrum of the continuum in the range up to 1 THz. The MPM also implies semi-empirical continuum modeling, which has a simpler functional form than MT_CKD. The construction of a physically based model of the continuum for the MPM in a narrower, but important for practical applications, spectral region is a much simpler task. Availability of results of measurements of collisional parameters of a number of the most intense H_2O lines, falling into this range and, which is especially important, the results of quantum chemical calculations of the water dimer spectrum [16] also contribute to its solution. The constructed continuum model will be further extended to the entire significant range of electromagnetic radiation.

DATA SELECTION

High-precision calculations of intensities of the vibrational-rotational lines of atmospheric gases have recently received much attention [17]. To test the results of these calculations, intensity measurements with comparable or higher accuracy are required. The spectral range under consideration is located in a poorly explored region between the microwave and infrared ranges. It is known as the "terahertz gap", in which measurements are difficult mainly due to the lack of good radiation sources and receivers (see, for example, the reviews [18, 19]). The lines of purely rotational transitions of a water molecule in various vibrational states fall into this region. Regular measurements of line intensities have not been made in the frequency range up to 1.75 THz. An exception is the results of microwave studies of three lines, which will be presented below. The most accurate measurements of the line intensities of rotational transitions of H_2O in the ground vibrational state and transitions from the ground to excited low-lying vibrational states were performed using Fourier spectrometers in higher frequency ranges (see [20] and references therein). The measurement error for the strongest lines was 3–5% in this case, increasing up to 20–30% for weak ones. The line intensity calculations by the method of effective Hamiltonians [20–22] based on these measurements (tens of purely rotational transitions and thousands of vibrational-rotational transitions belonging to the bands of fundamental vibrations and their combinations) allow averaging the inevitable statistical and systematic experimental errors. There are reasons to believe that these calculations predict line intensities (for the bands for which the experimental data are known) with an accuracy higher than the experimental one. However it cannot be guaranteed that this accuracy is much less than the scatter of the experimental data, which is also 3–5% (see [21, Figs. 4 and 6] and [20, Fig. 5]). Many spectroscopic applications require a higher accuracy.

An alternative high-precision method for calculating line intensities based on variational calculations was described in [23], where the average deviation of the calculated values from the experimental ones was 1–2% for some rotational-vibrational bands (including the purely rotational one). The ultimate capabilities of the method can be determined only by comparison with the results of special-purpose high-precision experiments that are currently available in the IR and visible ranges (see, for example, [17, 24], where intensity measurements with an uncertainty of ~ 0.01% were demonstrated). The average deviation of the results from the experiment (0.4% with a spread of 0.6% with experimental uncertainty ~ 0.4%) was shown in [25] based on the results of high-precision measurements of 15 intense lines of H_2O at about 7200 cm^{-1}. However, later measurements in other rotational-vibrational H_2O bands in the same frequency range [26] differed from the results of [25] by up to 5%. Improved calculations [27] enabled the achievement of a deviation of less than 1%, even with the measurements made in [26]. The results of subsequent careful comparison of theoretical predictions and measurement data showed that there was no satisfactory (~1%) agreement in all bands. In particular, it was found that, even for the transitions to states with highly excited stretching vibrations (which, according to the measurements [28, 29], are calculated better than bending vibrations), observed in the near-IR and visible ranges, the discrepancy between theory and measurements is ~ 2%. Further development of methods for calculating the line intensities of the H_2O molecule demonstrated a sub-percentage agreement with measurements of the $2\nu_1 + \nu_3$ band line at 10670 cm^{-1} [30]. In [23], where this method was proposed, it was noted that the intensity of most lines of the ground and

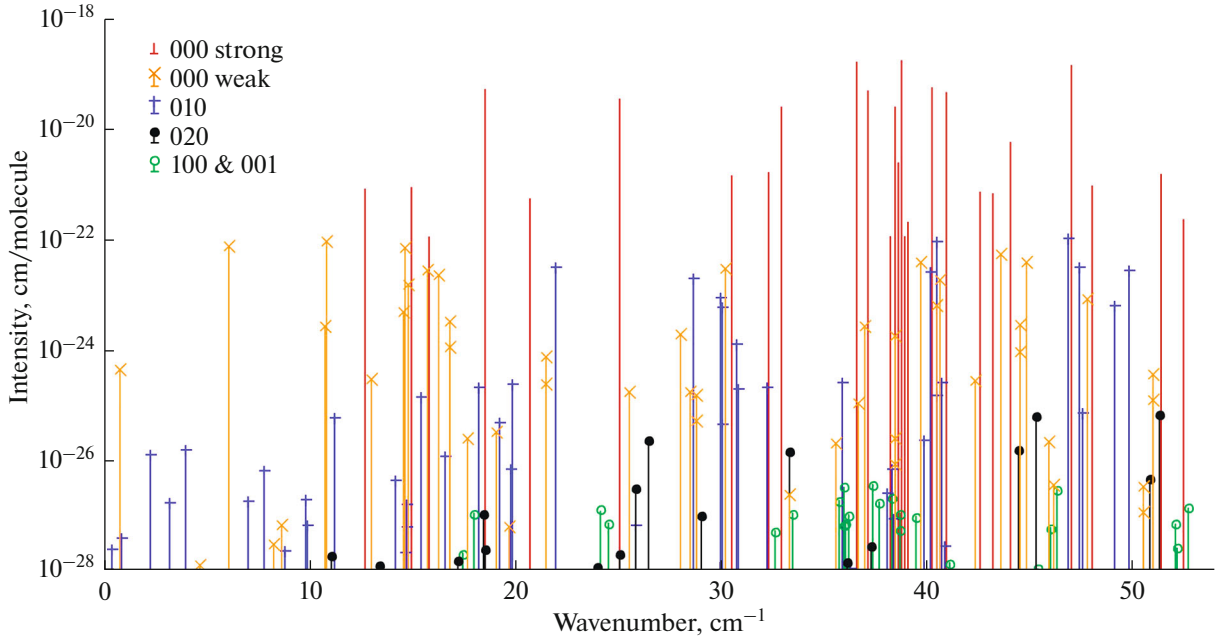

Fig. 1. Stick diagram of the considered spectrum.

low-lying vibrational states weakly depends on the empirical correction of the potential energy and dipole moment surfaces underlying the calculation.

Does the above mean that the intense lines of the H_2O molecule rotational band are calculated with an error of less than 1%? To answer this question, we analyzed all the absorption lines of the $H_2{}^{16}O$ molecule with an intensity of more than 10^{-28} cm/molecule falling in the 0–1.75 THz range. There were 161 such lines total. The lines were sorted as follows:

The most intense transitions (more than 10^{-22} cm/molecule) were selected. They actually determine the shape of the observed absorption spectrum of the atmosphere in the considered range. These lines correspond to 26 rotational transitions in the ground vibrational state.

For adequate comparison of the lines from the above list with their analogs in the ν_2 fundamental bending vibrational state, we took into account the intensity decrease associated with the population of the lower level (the Boltzmann factor equal to 4.3×10^{-4}), and selected all lines in the ν_2 state with intensity more than 4.3×10^{-26} cm/molecule. There were 23 such lines in the specified range.

For rotational lines in the $2\nu_2$, ν_1 and ν_3 vibrational states, a similar overall intensity decrease more than seven orders of magnitude. This means that all lines in these states (there were 17, 12, and 12 of them, respectively) can be used for comparison with the strong lines in the ground state.

The remaining weaker 48 lines in the ground state and 23 lines in the ν_2 state were used to estimate the uncertainty of the calculated intensity within a one vibrational state. The frequencies, intensities, and rotational quantum numbers of the selected lines are presented in Tables 1–5. A stick-diagram of the considered spectrum is shown in Fig. 1.

The intensities of the selected lines were taken from various public sources. They include information from the HITRAN [10, 31], GEISA [32, 33], and JPL [34] databases (in this work, these lists are conventionally designated as HIT20, GEI15, JPL12, respectively; the numbers indicate the year when they were published), and ExoMol [35, 36]. In the HITRAN database the calculated parameters of the lines are given in the considered frequency range. The frequencies correspond to [37], and the intensities are taken from [38]. These intensities were obtained by variational methods using the CKAPTEN quantum chemical dipole moment surface (DMS) [27] and the potential energy surface (PES) [39], which was additionally modified based on empirical information about molecular energy levels. The GEISA database contains the result of modeling empirical data on the H_2O spectrum by the method of effective Hamiltonians [22]. Note that the frequencies and intensities of the main isotopologue of the water molecule in the considered range in the GEISA-2020 remained unchanged compared to the database version of 2015. The list of lines from the JPL database is the result of [20]. It is also based on the use of effective Hamiltonians and known experimental data. The ExoMol database contains several spectra of the water molecule obtained by variational methods: 1) BT2 [40] (BT206), calculated using a semi-empirical PES from [41] and two quantum-chemical DMSs from [23] and [42]; 2) POKAZATEL

Table 1. Relative deviation, in percent, of the calculated intensity from the mean value (I_{av}, cm/molecule) for $J'_{Ka',\ Kc'} \leftarrow J_{Ka,\ Kc}$ rotational transitions in the ground state

Transition	ν, cm^{-1}	I_{av}	HIT20	GEI15	JPL12	POK18	BT206	WAT20	Bub11	Miz18
$3_{2,1} - 3_{1,2}$	38.791	1.765e-19	0.72	0.09	−1.63	−0.34	1.24	−0.29	0.71	0.74
$3_{1,2} - 3_{3,0}$	36.604	1.618e-19	0.78	0.11	−1.85	−0.29	1.25	−0.35	0.80	0.81
$5_{2,3} - 5_{1,4}$	47.053	1.407e-19	0.35	−0.48	−0.68	0.08	1.64	0.08	0.32	0.34
$4_{2,2} - 4_{1,3}$	40.283	5.515e-20	0.55	−0.16	−1.20	−0.14	1.40	−0.14	0.54	0.56
$1_{1,0} - 1_{1,0}$	18.577	5.184e-20	1.01	0.41	−2.36	−0.55	0.99	−0.53	1.00	1.02
$1_{1,1} - 0_{0,0}$	37.137	4.946e-20	1.03	0.45	−2.42	−0.55	0.94	−0.57	1.02	1.04
$2_{2,0} - 2_{1,1}$	40.988	4.752e-20	0.85	0.28	−1.95	−0.45	1.08	−0.43	0.84	0.86
$2_{1,1} - 2_{2,0}$	25.085	3.421e-20	0.91	0.29	−2.15	−0.44	1.08	−0.47	0.92	0.94
$3_{1,2} - 2_{2,1}$	38.464	2.507e-20	0.75	0.42	−1.81	−0.32	1.11	−0.44	0.71	0.69
$2_{2,0} - 1_{1,1}$	32.954	2.488e-20	0.94	0.44	−2.28	−0.45	0.99	−0.53	0.94	0.94
$6_{2,5} - 5_{3,2}$	44.099	5.698e-21	−0.14	0.51	0.01	−0.04	1.38	−0.02	−0.16	−0.17
$6_{3,4} - 5_{4,1}$	38.638	2.446e-21	−0.39	0.49	0.60	0.16	1.50	−0.01	−0.40	−0.45
$5_{2,4} - 4_{3,1}$	32.366	1.601e-21	0.14	0.51	−0.56	−0.13	1.30	−0.19	0.14	0.11
$6_{3,3} - 5_{4,2}$	51.435	1.531e-21	−0.35	0.41	0.58	0.17	1.60	0.04	−0.40	−0.44
$4_{2,2} - 3_{3,1}$	30.560	1.420e-21	0.37	0.43	−1.04	−0.11	1.23	−0.32	0.35	0.30
$7_{2,6} - 6_{3,3}$	48.059	9.396e-22	−0.50	0.57	0.75	0.05	1.45	0.15	−0.51	−0.50
$4_{2,3} - 3_{3,0}$	14.944	8.598e-22	0.38	0.49	−1.08	−0.09	1.16	−0.31	0.35	0.26
$4_{1,4} - 3_{2,1}$	12.682	8.214e-22	0.55	0.53	−1.50	−0.36	0.91	−0.25	0.54	0.50
$7_{4,3} - 6_{5,2}$	42.638	7.219e-22	−1.03	0.48	2.06	0.46	1.80	0.22	−1.06	−1.13
$8_{2,7} - 7_{3,4}$	43.244	6.993e-22	−0.94	0.69	1.63	0.13	1.55	0.35	−0.95	−0.92
$5_{3,2} - 4_{4,1}$	20.704	5.676e-22	−0.10	0.50	−0.01	0.16	1.44	−0.18	−0.13	−0.24
$6_{4,3} - 7_{1,6}$	52.511	2.291e-22	−0.87	1.43	1.55	−0.22	1.39	−0.18	−0.89	−0.83
$7_{4,4} - 6_{5,1}$	39.111	2.017e-22	−1.04	0.51	2.07	0.43	1.76	0.23	−1.06	−1.13
$7_{2,5} - 8_{1,8}$	38.247	1.145e-22	−0.98	1.57	1.58	−0.03	1.63	−0.29	−0.95	−0.90
$8_{5,4} - 7_{6,1}$	38.972	1.129e-22	−1.79	0.50	3.82	0.77	2.01	0.50	−1.86	−1.95
$5_{3,3} - 4_{4,0}$	15.834	1.091e-22	−0.07	0.49	−0.04	0.21	1.31	−0.16	−0.15	−0.28
		dI_{av}	0.04	0.46	−0.30	−0.07	1.35	−0.16	0.03	0.01
		RMSD	0.78	0.38	1.65	0.32	0.28	0.28	0.78	0.80

[39] (POK18), derived from the PES from [43], which was further optimized to better describe the known data, and the quantum chemical DMS, known as LPT2011s [25]; 3) WAT-UV296 [44] (WAT20), which used a combined PES based on surfaces from [39] and [43] and CKAPTEN DMS. In addition, we considered the results of two quantum-chemical calculations of the line intensities from [46], which differ in used PES. In one case (Bub11), the semi-empirical the PES from [43] was used, and in the second (Miz18) the PES was additionally empirically modified. In both cases, the LPT2011 DMS was used [25]. In addition to the calculated values, for comparison, we used the results of measuring the line intensities at 0.74 [46, 47], 6.11 [48], and 10.8 cm^{-1} [49]. The line intensities from all sources were reduced to cm/molecule units at 296 K and 100% isotopologue content of $H_2{}^{16}O$.

ANALYSIS

As a first approximation of the most probable intensity value, it is proposed to take the arithmetic mean of all calculated intensity values from different sources for each line. Further reasoning is based on the analysis of the differences between the result of each particular calculation and the average value.

For the strongest transitions of the ground vibrational state (Table 1), the intensity deviations calculated in this way turned out to be mainly less than 1%. Note that we have not found the dependence of the

magnitude of deviations on the rotational quantum numbers of intense transitions either for the ground or the considered excited vibrational states. For almost every data source, the deviation of intensities from the mean I_{av} is sign-alternating. Therefore, the systematic error does not dominate. The exception is the BT206 list, with an average deviation of 1.35%. For this reason, BT206 was excluded from the calculation of the average values in Table 1. Experimental data were not used either. The results of comparing the intensities are summarized in the last two rows of Table 1 as a mean intensity deviation from the average (dI_{av}), and a root mean square deviation (RMSD) characterizing the systematic overestimation or underestimation of data for each source.

For almost all sources, the absolute value of the average deviation and the RMSD are less than 0.5 and 0.8%, respectively. The exceptions are the aforementioned earliest BT206 variational calculation (systematically overestimating the intensity by 1.35%) and the calculation by the method of effective Hamiltonians JPL12 (the spread of values is about 2%). The difference between the Bub11 and Miz18 is due only to a minor modification of the PES and is less than 0.1%. This means that the result of additional empirical modification of the PES has little effect on the wave functions of the ground state levels. To analyze the lines belonging to all other vibrational states considered in this paper, we will not use the Bub11 list, which is regarded to be less accurate [45].

The transitions within the ν_2 bending vibrational state with an energy of ~ 1600 cm^{-1} are shown in Table 2. It can be seen that the standard deviations of the data from different sources are comparable with the values of the standard deviations for the ground vibrational state. The deviations from the mean value are noticeably larger than for the ground state and become strictly sign-constant for each source. Exclusion of any source results in a significant shift in the mean value. The largest deviation (for any method of determining the mean value) is for JPL12. In fact, JPL12 is a previous version of a more accurate GEI15 calculation, which was obtained by the same method, but involving new experimental data. Therefore, JPL12 data were not used in further analysis for the mean value calculation. The POK18 and WAT20 data seem to be the best for the ν_2 state with a slight advantage of POK18.

The transitions in the $2\nu_2$ vibrational state with energy ~ 3200 cm^{-1} are listed in Table 3 and the transitions in the ν_1 and ν_3 states with the energy of the lower levels ~ 3700 cm^{-1} in Table 4. The data from Tables 3 and 4 can be divided into three groups: the intensities of GEI15, Miz18, and HIT20 are systematically 7–9% lower than the average value; the intensities of JPL12 are 12–20% higher; and BT206, POK18, and WAT20 all had an overall average deviation of 2–5%. Such a large data scatter results in an even lower reliability of the estimates based on the calculation of the mean value of intensities. Interestingly, the standard deviations for all vibrational states are close; therefore, the rotational part in the calculations of the intense lines is taken into account correctly, and the error is due only to the vibrational part of the potential and the corresponding wave functions.

Information from Tables 1–4 on the deviations of the calculated intensities from the mean value versus the line intensity is presented in Fig. 2.

A decrease in the accuracy of the calculated data (systematic deviation from the mean value) with an increase in the energy of the lower level of the transition or vibrational excitation of the molecule is expected and explained as follows. To calculate the transition matrix element of the dipole moment determining line intensity, the product of the dipole moment and the wave functions of the lower and upper states should be integrated. The corresponding region of integration is determined by intramolecular spatial configurations, in which the values of the wave functions differ significantly from zero. For the transitions in the ground vibrational state, the region of significant values of the wave functions and dipole moments is in the neighborhood of the equilibrium configuration of the molecule. With an increase in the internal energy, the region of space that is significant for the integration expands and the accuracy of the wave functions in variational calculations and the specific features of the particular PES and DMS used to calculate the transition matrix elements begin to strongly influence the result of integration. As a consequence, the scatter of the results increases, and their reliability reduces.

Based on the data presented, it can be assumed that for the strongest transitions in the ground vibrational state, all calculations provide comparable accuracy in calculating the line intensity with an average uncertainty of 1–2%. The discrepancy between the results indicating a decrease in the accuracy of the calculations increases with increasing vibrational excitation reaching up to ~ 10% for the lines in the ν_1 and ν_3 states. Moreover, for the ν_2 and $2\nu_2$ states one can see a systematic discrepancy between the calculations as the intensity of the lines decreases (Fig. 2). To make sure that this trend is a general pattern, we compared the results of the calculations for all other less intense lines (from 10^{-22} to 10^{-28} cm/molecule) of the ground state falling within the considered frequency range (Table 5). The result of this analysis together with the data from Table 1 are shown in Fig. 3.

It can be seen that the difference between the calculations, indeed, increases as the line intensity decreases. For the method of effective Hamiltonians, this is apparently a consequence of the lack of reliable empirical information about low-intensity lines. In the case of variational calculations, the error is associated with the imperfection of the used PES, which leads, in

Table 2. The same as Table 1 for the ν_2 vibrational state

Transition	ν, cm^{-1}	I_{av}	HIT20	GEI15	JPL12	POK18	BT206	WAT20	Bub11
$3_{1,2} - 3_{0,3}$	40.517	8.963e-23	−3.08	−1.90	6.79	0.97	2.47	0.93	−3.07
$4_{2,2} - 4_{1,3}$	47.431	3.133e-23	−3.39	−2.25	7.45	1.16	2.65	1.09	−3.38
$1_{1,0} - 1_{0,1}$	21.949	3.101e-23	−2.89	−1.58	6.25	0.81	2.28	0.77	−2.85
$2_{2,0} - 2_{1,1}$	49.836	2.805e-23	−3.05	−1.77	6.66	0.92	2.41	0.85	−3.05
$1_{1,1} - 0_{0,0}$	40.221	2.488e-23	−2.85	−1.52	6.18	0.78	2.30	0.74	−2.82
$2_{1,1} - 2_{0,2}$	28.685	1.961e-23	−2.98	−1.71	6.47	0.88	2.30	0.83	−2.94
$2_{0,2} - 1_{1,1}$	29.997	8.482e-24	−2.88	−1.56	6.34	0.76	2.27	0.80	−2.90
$5_{2,3} - 4_{3,2}$	49.153	6.287e-24	−3.78	−2.00	8.07	0.95	2.50	1.06	−3.83
$3_{1,2} - 2_{2,1}$	30.108	5.967e-24	−3.10	−1.67	6.84	0.79	2.36	0.89	−3.14
$6_{2,5} - 5_{3,2}$	30.792	1.227e-24	−4.16	−2.06	8.60	0.95	2.41	1.11	−4.23
$7_{2,6} - 6_{3,3}$	35.950	2.547e-25	−4.68	−2.23	9.25	1.06	2.43	1.17	−4.69
$7_{3,5} - 6_{4,2}$	40.789	2.463e-25	−4.79	−2.39	9.94	1.11	2.65	1.28	−4.87
$6_{3,4} - 5_{4,1}$	19.850	2.339e-25	−4.29	−2.16	9.32	0.91	2.49	1.25	−4.42
$5_{2,4} - 4_{3,1}$	18.236	2.092e-25	−3.75	−1.90	8.08	0.81	2.28	1.09	−3.83
$8_{2,7} - 7_{3,4}$	32.291	2.056e-25	−5.27	−2.39	10.02	1.12	2.43	1.27	−5.22
$6_{3,3} - 5_{4,2}$	30.894	1.952e-25	−4.30	−2.22	9.29	1.01	2.59	1.21	−4.43
$8_{4,5} - 7_{5,2}$	40.530	1.501e-25	−5.57	−2.79	11.54	1.29	2.82	1.49	−5.67
$4_{2,2} - 3_{3,1}$	15.450	1.368e-25	−3.33	−1.79	7.68	0.71	2.39	1.08	−3.48
$8_{4,4} - 7_{5,3}$	47.649	6.961e-26	−5.56	−2.81	11.56	1.32	2.88	1.49	−5.66
$5_{2,3} - 6_{1,6}$	11.215	5.665e-26	−4.02	−1.63	8.36	1.02	2.81	0.61	−3.96
$7_{4,3} - 6_{5,2}$	19.282	4.782e-26	−4.93	−2.51	10.86	1.05	2.74	1.46	−5.15
$6_{2,4} - 7_{1,7}$	30.101	4.386e-26	−4.52	−1.69	9.06	0.95	2.56	0.74	−4.48
		dI_{av}	−3.93	−2.02	8.33	0.97	2.50	1.05	−3.97
		RMSD	0.88	0.37	1.65	0.16	0.18	0.25	0.91
$9_{5,4} - 8_{6,3}$	39.922	2.232e-26	−6.45	−3.27	13.50	1.52	3.04	1.75	−6.60
$2_{2,0} - 3_{1,3}$	4.0026	1.477e-26	−3.79	−1.15	6.56	1.01	2.50	0.14	−3.52
$4_{1,4} - 3_{2,1}$	2.2617	1.273e-26	−2.56	−2.56	7.55	1.02	1.57	1.54	−2.96
$7_{4,4} - 6_{5,1}$	16.628	1.184e-26	−4.89	−2.50	10.85	1.00	2.68	1.50	−5.15
$9_{2,8} - 8_{3,5}$	19.804	6.951e-27	−5.95	−2.59	10.89	1.20	2.25	1.39	−5.90
$9_{5,5} - 8_{6,2}$	38.334	6.860e-27	−6.45	−3.25	13.52	1.51	3.06	1.74	−6.59
$5_{5,0} - 6_{4,3}$	7.7616	6.520e-27	−5.40	−2.91	10.27	1.95	3.07	0.96	−4.92
$8_{5,4} - 7_{6,1}$	14.199	4.347e-27	−5.67	−2.93	12.70	1.16	2.86	1.76	−6.01
$10_{6,5} - 9_{7,2}$	38.078	2.458e-27	−7.46	−3.82	15.78	1.79	3.37	2.03	−7.61
$6_{6,1} - 7_{5,2}$	9.7956	1.909e-27	−6.00	−3.59	12.20	2.21	3.36	1.38	−5.54
$5_{5,1} - 6_{4,2}$	6.9754	1.758e-27	−5.62	−2.72	10.11	1.90	2.98	0.82	−5.07
$4_{4,0} - 5_{3,3}$	3.2109	1.610e-27	−5.59	−1.86	8.51	1.25	3.08	0.61	−4.69
$8_{5,3} - 7_{6,2}$	14.701	1.553e-27	−5.64	−2.91	12.72	1.17	2.90	1.75	−6.00
$10_{6,4} - 9_{7,3}$	38.379	8.323e-28	−7.45	−3.83	15.79	1.79	3.37	2.04	−7.62
$6_{6,0} - 7_{5,3}$	9.9215	6.526e-28	−5.98	−3.62	12.21	2.24	3.35	1.38	−5.53
$10_{3,7} - 11_{2,10}$	25.846	6.409e-28	−6.85	−2.49	13.57	1.36	3.23	1.13	−6.86
$9_{6,3} - 8_{7,2}$	14.718	6.258e-28	−6.61	−3.47	14.86	1.43	3.15	2.05	−7.00
$5_{3,2} - 4_{4,1}$	0.8951	3.727e-28	2.02	−3.67	10.14	0.57	1.24	3.10	−1.57
$11_{7,4} - 10_{8,3}$	40.895	2.743e-28	−7.76	−6.30	19.42	3.04	4.61	3.26	−7.94
$4_{2,3} - 3_{3,0}$	0.4006	2.392e-28	5.68	−5.10	9.95	0.45	−1.10	4.65	0.53
$7_{7,0} - 8_{6,3}$	8.7878	2.273e-28	−6.81	−4.52	14.48	2.77	3.78	1.76	−6.24
$9_{6,4} - 8_{7,1}$	14.634	2.049e-28	−5.98	−4.81	15.62	2.09	3.84	2.72	−6.38
$13_{3,11} - 12_{4,8}$	36.310	1.039e-28	−7.85	−6.49	17.54	3.15	4.11	3.34	−7.75

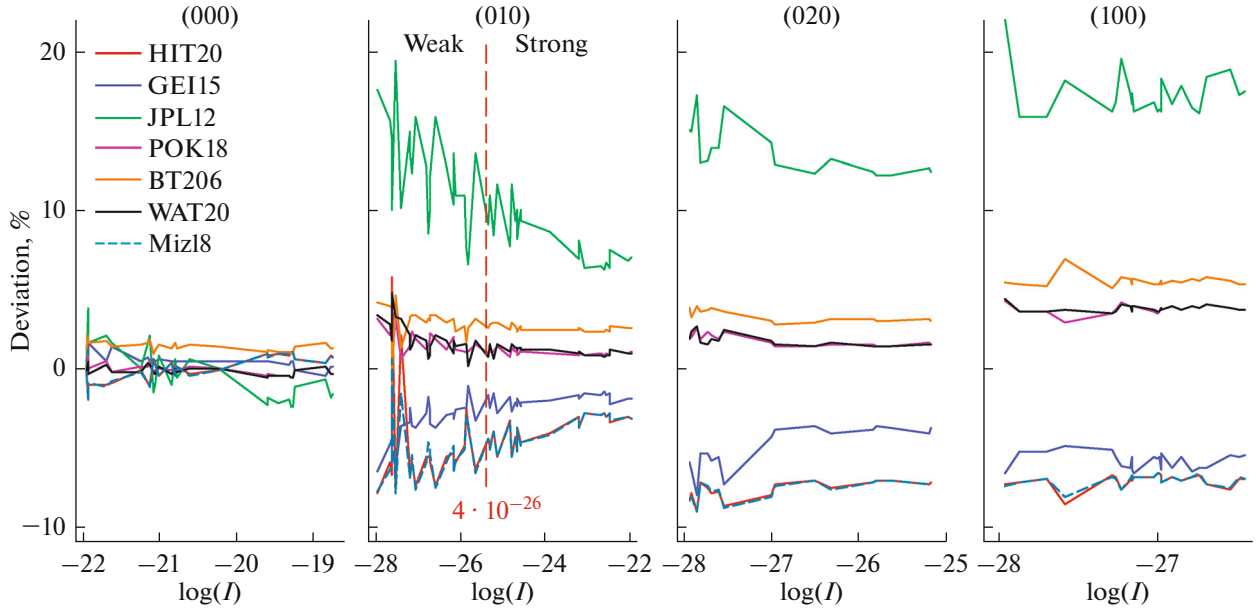

Fig. 2. Deviations of the line intensities from the mean value for different data sources and vibrational states versus the logarithm of the intensity (see Tables 1–4).

particular, to inaccuracies in determining wave functions. These inaccuracies have approximately the same absolute value for all rotational states, but their relative contribution is the greater the lower the calculated line intensity. This is most evident for the Miz18 and HIT20 calculations and to a lesser extent for BT206, POK18, and WAT20. Such a difference in the results of calculations cannot be explained by differences in the DMS. Thus, WAT20 disagrees with HIT20, which was obtained with the same DMS

Table 3. The same as Table 1 for the $2\nu_2$ vibrational state

Transition	ν, cm^{-1}	I_{av}	HIT20	GEI15	JPL12	POK18	BT206	WAT20	Miz18
$3_{0,3} - 2_{1,2}$	51.325	6.454e-26	−7.27	−3.79	12.42	1.45	2.99	1.46	−7.27
$3_{1,2} - 3_{0,3}$	45.384	6.124e-26	−7.36	−4.10	12.60	1.56	3.15	1.51	−7.35
$1_{1,0} - 1_{0,1}$	26.472	2.317e-26	−7.11	−3.73	12.15	1.42	3.01	1.37	−7.10
$1_{1,1} - 0_{0,0}$	44.463	1.563e-26	−7.05	−3.68	12.09	1.38	2.97	1.38	−7.08
$2_{1,1} - 2_{0,2}$	33.385	1.398e-26	−7.24	−3.89	12.33	1.50	3.07	1.43	−7.21
$4_{1,3} - 3_{2,2}$	50.894	4.555e-27	−7.60	−4.09	13.18	1.54	3.05	1.56	−7.64
$2_{0,2} - 1_{1,1}$	25.868	3.095e-27	−7.12	−3.71	12.22	1.40	2.91	1.43	−7.15
$3_{1,2} - 2_{2,1}$	18.481	1.031e-27	−7.32	−3.90	12.89	1.43	2.78	1.53	−7.40
$5_{2,3} - 4_{3,2}$	29.056	9.445e-28	−8.02	−4.39	14.20	1.62	2.97	1.72	−8.10
$7_{3,4} - 6_{4,3}$	37.322	2.740e-28	−8.69	−7.30	16.53	2.28	3.59	2.35	−8.77
$3_{3,0} - 4_{2,3}$	18.574	2.414e-28	−7.79	−5.56	13.82	1.87	3.69	1.67	−7.69
$5_{2,3} - 6_{1,6}$	25.063	1.966e-28	−7.88	−5.89	13.90	2.07	3.75	1.87	−7.83
$3_{2,1} - 4_{1,4}$	11.045	1.775e-28	−7.55	−5.35	13.05	2.26	3.61	1.47	−7.48
$2_{2,0} - 3_{1,3}$	17.220	1.449e-28	−7.24	−5.44	12.94	1.80	3.53	1.60	−7.18
$8_{3,6} - 7_{4,3}$	36.192	1.358e-28	−9.07	−7.97	17.14	2.51	3.90	2.58	−9.10
$6_{2,5} - 5_{3,2}$	13.440	1.186e-28	−7.94	−6.42	14.90	1.98	3.25	2.32	−8.08
$4_{4,1} - 5_{3,2}$	24.032	1.106e-28	−8.39	−5.95	15.02	2.00	3.81	1.82	−8.30
		dI_{av}	−7.68	−5.01	13.61	1.77	3.30	1.71	−7.69
		RMSD	0.57	1.31	1.48	0.35	0.36	0.36	0.58

Table 4. The same as Table 1 for the ν_1 and ν_3 vibrational states

VS	Transition	ν, cm^{-1}	I_{av}	HIT20	GEI15	JPL12	POK18	BT206	WAT20	Miz18
ν_1	$3_{1,2} - 3_{0,3}$	36.021	3.255e-27	−6.94	−5.61	17.18	3.63	5.29	3.63	−6.93
ν_1	$5_{2,3} - 5_{1,4}$	46.384	2.859e-27	−7.63	−5.54	18.84	3.81	5.55	3.81	−7.60
ν_3	$4_{2,2} - 4_{1,3}$	38.319	1.996e-27	−7.36	−6.30	18.29	3.99	5.69	3.99	−7.34
ν_3	$1_{1,1} - 0_{0,0}$	35.772	1.805e-27	−6.73	−6.32	16.06	3.80	5.45	3.80	−6.70
ν_3	$2_{2,0} - 2_{1,1}$	37.729	1.651e-27	−6.90	−6.52	16.43	3.91	5.60	3.91	−6.87
ν_1	$4_{1,3} - 4_{0,4}$	52.786	1.393e-27	−7.14	−5.62	17.78	3.71	5.35	3.71	−7.16
ν_3	$2_{1,1} - 2_{0,2}$	24.172	1.232e-27	−6.92	−6.29	16.65	3.84	5.54	3.84	−6.87
ν_1	$4_{2,2} - 4_{1,3}$	38.757	1.054e-27	−7.25	−5.35	18.21	3.66	5.27	3.66	−7.26
ν_3	$2_{0,2} - 1_{1,1}$	33.512	1.043e-27	−6.75	−6.38	16.21	3.81	5.53	3.81	−6.77
ν_1	$1_{1,0} - 1_{0,1}$	18.038	1.016e-27	−6.65	−5.66	16.32	3.55	5.22	3.55	−6.64
ν_1	$1_{1,1} - 0_{0,0}$	36.241	9.782e-28	−6.60	−5.70	16.19	3.49	5.22	3.59	−6.60
ν_1	$2_{2,0} - 2_{1,1}$	39.505	9.331e-28	−6.84	−5.58	16.78	3.57	5.23	3.62	−6.83
ν_3	$2_{2,1} - 2_{1,2}$	52.161	7.063e-28	−6.83	−6.65	16.20	3.93	5.62	3.93	−6.82
ν_3	$3_{2,1} - 3_{1,2}$	36.056	6.895e-28	−7.09	−6.40	17.26	3.93	5.61	3.95	−7.08
ν_1	$2_{1,1} - 2_{0,2}$	24.523	6.791e-28	−6.76	−5.64	16.66	3.57	5.23	3.59	−6.76
ν_3	$3_{1,2} - 3_{0,3}$	36.033	6.642e-28	−7.05	−6.26	17.34	3.86	5.60	3.86	−7.04
ν_3	$5_{2,3} - 5_{1,4}$	46.072	5.881e-28	−7.68	−6.23	19.51	4.08	5.78	4.05	−7.66
ν_1	$3_{1,2} - 2_{2,1}$	38.698	5.401e-28	−6.92	−5.56	16.77	3.67	5.24	3.58	−7.00
ν_1	$2_{0,2} - 1_{1,1}$	32.648	5.136e-28	−6.79	−5.18	16.19	3.46	5.06	3.45	−6.83
ν_3	$5_{3,2} - 5_{2,3}$	52.182	2.586e-28	−8.55	−4.88	18.06	2.92	6.90	3.62	−8.15
ν_3	$1_{1,0} - 1_{0,1}$	17.489	2.015e-28	−7.02	−5.23	15.86	3.52	5.20	3.52	−6.99
ν_3	$3_{1,2} - 2_{2,1}$	41.125	1.341e-28	−7.23	−5.29	15.79	3.60	5.31	3.60	−7.27
ν_1	$6_{2,5} - 5_{3,2}$	45.453	1.083e-28	−7.35	−6.70	22.05	4.29	5.39	4.38	−7.43
			dI_{av}	−7.08	−5.85	17.25	3.72	5.46	3.75	−7.07
			RMSD	0.41	0.51	1.39	0.26	0.35	0.21	0.36

(CKAPTEN), and agrees (for all considered vibrational states) with POK18, which was obtained with another DMS (LTPs). The agreement between Miz18 and HIT20 is even better although these calculations use different DMS. The systematically increasing deviation of the Miz18 and HIT20 calculations from the mean value with decreasing intensity is probably explained by the attempt of the authors to vary the PES parameters aimed at obtaining the best result in the frequency range with an upper limit (15000 cm^{-1} for Miz18 and 26000 cm^{-1} for HIT20). The BT206, POK18 and WAT20 calculations are regarded more global (for example, POK18 – up to the dissociation threshold). The corresponding PESs, on the average, describe the entire rotational-vibrational spectrum better and, as can be seen from the comparison, agree in the predictions of the line intensities in the ground state. A slight systematic shift in the results of BT206 relative to POK18 and WAT20 (virtually independent of either line intensity or vibrational state) is explained by the use of an earlier and, apparently, less accurate even for the considered states DMS. The difference between the LTP, LTPs, and CKAPTEN surfaces does not notably affect the intensity.

The difference between POK18 and WAT20, that are leading in our analysis, is sign-alternating for all states, which is about 0.1% on the average. However, we cannot assert that these results are true, with about the same uncertainty because no measurements have been made. Nevertheless, there is a good agreement between global variational calculations and GEI15, which are based on a huge amount of experimental data in the adjacent frequency range. These data include information on the line positions (providing accurate information on the wave functions of the states) and on the intensities of purely rotational and vibrational-rotational transitions (providing information on the parameters of the dipole moment). The above agreement cannot be accidental. It allows considering the GEI15 data as an analogue of the

Table 5. The same as Table 1 for less intense lines in the ground state

Transition	ν, cm^{-1}	I_{av}	HIT20	GEI15	JPL12	POK18	BT206	WAT20	Miz18
$8_{6,2} - 7_{7,1}$	16.828	1.085e-24	−2.29	0.55	4.89	1.13	2.05	0.58	−2.55
$10_{7,3} - 9_{8,2}$	44.564	9.146e-25	−3.70	0.44	8.23	1.41	2.71	1.17	−3.84
$9_{7,2} - 8_{8,1}$	21.545	7.289e-25	−3.19	0.52	7.08	1.38	2.37	0.91	−3.46
$6_{1,6} - 5_{2,3}$	0.7417	4.391e-25	1.37	−4.57	−0.43	−0.84	−5.03	2.02	0.94
$11_{8,3} - 10_{9,2}$	51.010	3.633e-25	−4.81	0.29	10.8	1.74	2.95	1.52	−4.70
$10_{3,7} - 11_{2,10}$	13.015	2.955e-25	−2.74	1.88	5.59	1.02	3.08	−0.23	−2.76
$13_{3,11} - 12_{4,8}$	42.412	2.699e-25	−4.20	1.10	8.64	1.12	2.27	1.67	−4.12
$9_{7,3} - 8_{8,0}$	21.540	2.429e-25	−3.20	0.52	7.08	1.39	2.38	0.90	−3.46
$11_{5,7} - 12_{2,10}$	25.578	1.712e-25	−3.86	1.99	8.08	0.71	2.52	0.71	−3.74
$12_{5,8} - 13_{2,11}$	28.488	1.705e-25	−4.61	2.17	9.67	0.99	2.80	0.87	−4.48
$10_{8,3} - 9_{9,0}$	28.815	1.468e-25	−4.23	0.44	9.56	1.63	2.72	1.29	−4.45
$11_{8,4} - 10_{9,1}$	51.006	1.211e-25	−4.78	0.28	10.80	1.72	2.95	1.55	−4.71
$11_{6,6} - 12_{3,9}$	36.730	1.065e-25	−4.25	2.03	9.09	0.64	2.32	0.92	−4.12
$10_{8,2} - 9_{9,1}$	28.815	4.894e-26	−4.22	0.43	9.54	1.66	2.70	1.29	−4.46
$12_{6,7} - 13_{3,10}$	19.077	3.227e-26	−5.00	1.96	10.6	0.83	2.62	1.23	−4.66
$11_{9,2} - 10_{10,1}$	38.532	2.458e-26	−5.32	0.28	12.2	1.97	3.11	1.73	−5.54
$14_{3,12} - 13_{4,9}$	17.690	2.396e-26	−5.11	1.36	10.4	0.96	1.63	2.38	−4.92
$14_{5,10} - 15_{2,13}$	45.971	2.060e-26	−6.21	2.58	13.3	1.43	3.03	1.24	−6.11
$13_{5,9} - 14_{2,12}$	35.647	2.039e-26	−5.37	2.36	11.4	1.23	2.94	1.03	−5.27
$11_{9,3} - 10_{10,0}$	38.532	8.192e-27	−5.33	0.28	12.3	1.98	3.39	1.71	−5.54
$13_{7,7} - 14_{4,10}$	46.241	3.405e-27	−6.27	2.32	13.6	1.12	2.64	1.53	−6.06
$12_{10,3} - 11_{11,0}$	50.571	3.324e-27	−6.53	0.01	15.1	2.31	3.48	2.13	−6.49
$15_{4,11} - 16_{3,14}$	33.388	2.336e-27	−7.96	1.34	13.7	0.76	2.56	0.08	−7.95
$12_{10,2} - 11_{11,1}$	50.571	1.108e-27	−6.51	−0.01	15.1	2.33	3.50	2.15	−6.50
$13_{6,8} - 14_{3,11}$	8.6711	6.306e-28	−4.99	−2.95	13.4	1.77	4.16	2.17	−4.37
$14_{7,8} - 15_{4,11}$	19.737	6.011e-28	−7.06	2.01	15.4	1.24	2.88	2.07	−6.59
$14_{4,10} - 15_{3,13}$	8.2537	2.863e-28	−5.30	−1.15	13.9	3.15	6.39	0.19	−5.49
$14_{6,9} - 15_{3,12}$	4.6570	1.263e-28	−6.79	−3.39	14.4	1.01	4.49	0.70	−5.89

experimental data for comparison with the results of variational calculations. In this case, the estimation of the line intensity uncertainty is the deviation of the variational calculations from these data. For the POK18 calculation leading in our study, this deviation is 0.06% on the average, no higher than 2% for almost all considered lines of the ground vibrational state with an intensity of more than 10^{-27} cm/molecule, and does not exceed 1% for lines with an intensity of more than 10^{-21} cm/molecule, the deviation (inset in Fig. 3). Note that for such strong lines, the deviation from the mean value does not exceed 1% for all the considered sources (excluding the least reliable JPL12 and BT206) (Fig. 2).

All results of experimental studies which we found in the literature are presented in Fig. 3. They correspond to intensity measurements of the three most important diagnostic atmospheric lines near 22, 183 and 325 GHz (0.74, 6.11 and 10.8 cm^{-1}), performed using resonator spectrometers. The measured intensities agree with the average calculated values within the doubled statistical error of the corresponding measurement,

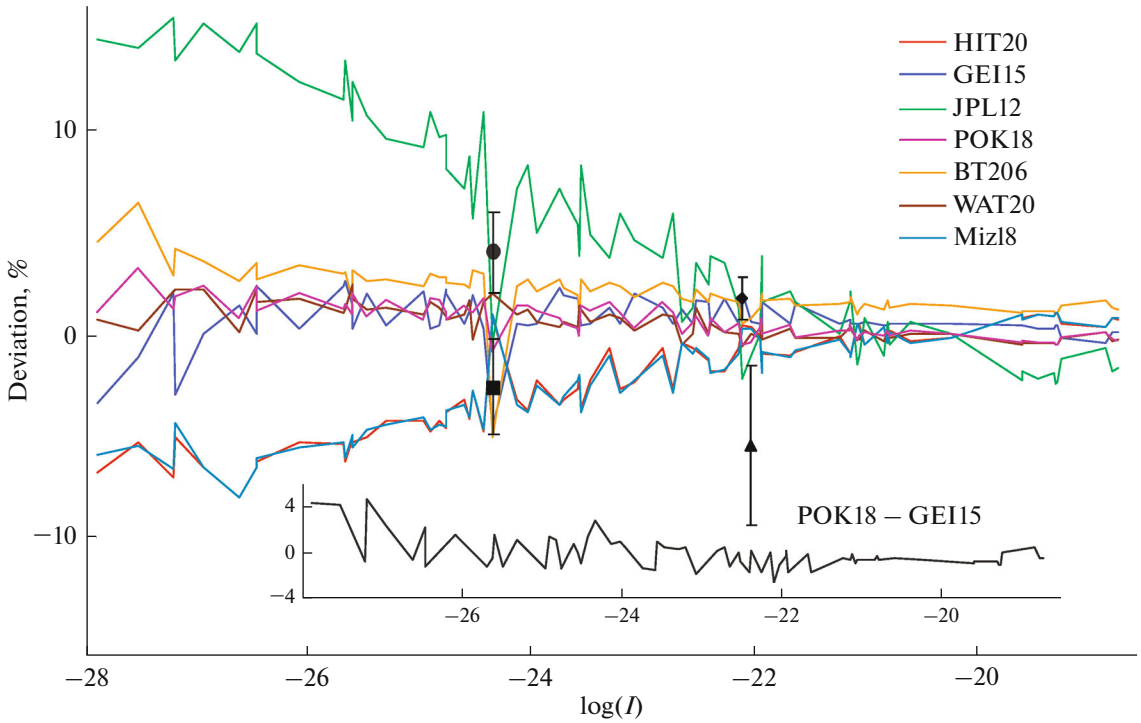

Fig. 3. Deviation of the calculated intensity of lines of the ground vibrational state from the mean value versus the logarithm of the intensity. The square, circle, rhombus, and triangle represent, respectively, the experimental data from [46–49]. The inset shows the difference between POK18 and GEI15 data.

which can be considered a good agreement given the complexity of such measurements.

For MPM users we add that the calculation of resonant absorption and moisture-related continuum in the 2022 version of this model is made on the basis of H_2O line intensities corresponding to HIT20. The potential error of these data can be estimated using Fig. 3.

CONCLUSIONS

Summarizing the results of the analysis we can say that in the considered frequency range the uncertainty of the calculated intensity of the rotational lines of the H_2O molecule in the ground vibrational state is from 1 to 2% for the intensity range from 10^{-21} to 10^{-27} cm/molecule, less than 1% for more intense and 5–10% for less intense lines. The exception is the line at 0.74 cm^{-1} with intensity 4.39×10^{-25} cm/molecule. The corresponding data points look like outliers on almost all graphs in Fig. 3. It is quite possible that this line belongs to the so-called "unstable" lines, for which small variations in PES and DMS parameters lead to significant changes in intensity. Indeed, the POK18 and WAT20 calculations, which are in good agreement with each other in all other cases (RMSD of the difference is 0.6%), differ for this line by almost 3%. Another potential source of the problem may be the low frequency of this line, for which the errors in the calculation of energy levels by variational methods become significant. Recall that in the frequency range under consideration, the intensity is proportional to the square of the line frequency, and the average error in calculating the energy levels by variational methods is about 0.01 cm^{-1}. The available calculated and experimental data show that the error in the intensity of this line ranges from 2 to 5%.

For the strong (over 10^{-26} cm/molecule) lines in the ν_2 state the uncertainty is 2–5% and increases to 5–10% for weak ones. For all lines in the $2\nu_2$, ν_1 and ν_3 states uncertainty is 5–10%.

Note that according to the HITRAN estimate for the ground vibrational state the intensity uncertainty is 2–5% for all lines with intensity greater than 10^{-27} cm/molecule. The same uncertainty is indicated for the ν_2 state. For all less intense lines in the ground state and lines in the other vibrational states considered in this work HITRAN gives an error of ~ 20%. Our estimates show that most of these lines can be assigned a higher (by 1–2 steps according to the HITRAN classification) intensity accuracy category which can be determined for each particular line based on the available data. The most reliable estimate of the most probable line intensity is the average between the GEI15, POK18 and WAT20 calculations.

ACKNOWLEDGMENTS

The authors are grateful to O.L. Polyansky and N.F. Zobov for reading the manuscript and valuable comments.

FUNDING

This work was supported by the Russian Science Foundation (no. 22-72-10118). The experimental data used for the H_2O lines near 183 and 325 GHz were obtained using the CKP-7 equipment (UNU no. 3589084).

CONFLICT OF INTEREST

The authors of this work declare that they have no conflicts of interest.

REFERENCES

1. D. Cimini, P. W. Rosenkranz, M. Yu. Tretyakov, M. A. Koshelev, and F. Romano, "Uncertainty of atmospheric microwave absorption model: impact on ground-based radiometer simulations and retrievals," Atmos. Chem. Phys. **18**, 15231–15259 (2018).
2. A. O. Koroleva, S. Kassi, and A. Campargue, "The water vapor self-continuum absorption at room temperature in the 1.25 μm window," J. Quant. Spectrosc. Radiat. Transfer **286**, 108206 (2022).
3. E. J. Mlawer, V. H. Payne, J. L. Moncet, J. S. Delamere, M. J. Alvarado, and D. C. Tobin, "Development and recent evaluation of the MT_CKD model of continuum absorption," Philos. Trans. R. Soc. A. Math. Phys. Eng. Sci. **370**, 2520–2556 (2012).
4. http://rtweb.aer.com/continuum_frame.html. Cited February 15, 2023.
5. I. V. Ptashnik, K. P. Shine, and A. A. Vigasin, "Water vapour self-continuum and water dimers: 1. Analysis of recent work," J. Quant. Spectrosc. Radiat. Transfer **112**, 1286–1303 (2011).
6. M. Yu. Tretyakov, M. A. Koshelev, E. A. Serov, V. V. Parshin, T. A. Odintsova, and G. M. Bubnov, "Water dimer and the atmospheric continuum," Phys.-Uspekhi **57** (11), 1083–1098 (2014).
7. T. A. Odintsova, M. Yu. Tretyakov, A. A. Simonova, I. V. Ptashnik, O. Pirali, and A. Campargue, "Measurement and temperature dependence of the water vapor self-continuum between 70 and 700 cm^{-1}," J. Mol. Struct. **1210**, 128046 (2020).
8. A. A. Simonova, I. V. Ptashnik, J. Elsey, R. A. McPheat, K. P. Shine, and K. M. Smith, "Water vapour self-continuum in near-visible IR absorption bands: Measurements and semiempirical model of water dimer absorption," J. Quant. Spectrosc. Radiat. Transfer **277**, 107957 (2022).
9. T. A. Odintsova, A. O. Koroleva, A. A. Simonova, A. Campargue, and M. Yu. Tretyakov, "The atmospheric continuum in the "terahertz gap" region (15–700 cm^{-1}): Review of experiments at SOLEIL synchrotron and modeling," J. Mol. Spectrosc. **386**, 111603 (2022).
10. I. E. Gordon, L. S. Rothman, R. J. Hargreaves, R. Hashemi, E. V. Karlovets, F. M. Skinner, E. K. Conway, C. Hill, R. V. Kochanov, Y. Tan, P. Wcislo, A. A. Finenko, K. Nelson, P. F. Bernath, M. Birk, V. Boudon, A. Campargue, K. V. Chance, A. Coustenis, B. J. Drouin, J.-M. Flaud, R. R. Gamache, J. T. Hodges, D. Jacquemart, E. J. Mlawer, A. V. Nikitin, V. I. Perevalov, M. Rotger, J. Tennyson, G. C. Toon, H. Tran, V. G. Tyuterev, E. M. Adkins, A. Baker, A. Barbe, E. Cane, A. G. Csaszar, A. Dudaryonok, O. Egorov, A. J. Fleisher, H. Fleurbaey, A. Foltynowicz, T. Furtenbacher, J. J. Harrison, J.-M. Hartmann, V.-M. Horneman, X. Huang, T. Karman, J. Karns, S. Kassi, I. Kleiner, V. Kofman, F. Kwabia-Tchana, N. N. Lavrentieva, T. J. Lee, D. A. Long, A. A. Lukashevskaya, O. M. Lyulin, V. Yu. Makhnev, W. Matt, S. T. Massie, M. Melosso, S. N. Mikhailenko, D. Mondelain, H. S. P. Muller, O. V. Naumenko, A. Perrin, O. L. Polyansky, E. Raddaoui, P. L. Raston, Z. D. Reed, M. Rey, C. Richard, R. Tobias, I. Sadiek, D. W. Schwenke, E. Starikova, K. Sung, F. Tamassia, S. A. Tashkun, Auwera J. Vander, I. A. Vasilenko, A. A. Vigasin, G. L. Villanueva, B. Vispoel, G. Wagner, A. Yachmenev, and S. N. Yurchenko, "The HITRAN2020 molecular spectroscopic database," J. Quant. Spectrosc. Radiat. Transfer **277**, 107949 (2022).
11. A. O. Koroleva, T. A. Odintsova, M. Yu. Tretyakov, O. Pirali, and A. Campargue, "The foreign-continuum absorption of water vapour in the far-infrared (50–500 cm^{-1})," J. Quant. Spectrosc. Radiat. Transfer **261**, 107486 (2021).
12. H. J. Liebe, "MPM—an atmospheric millimeter wave propagation model," Intern. J. Infrared. Mill. Waves **10**, 631–650 (1989).
13. P. W. Rosenkranz, "Line-by-line microwave radiative transfer (non-scattering)," Remote Sens. Code Library (2017). https://doi.org/10.21982/M81013
14. http://cetemps.aquila.infn.it/mwrnet/lblmrt_ns.html. Cited February 15, 2023.
15. S. A. Clough, F. X. Kneizys, and R. W. Davies, "Line shape and water vapor continuum," Atmos. Res. **23**, 229–241 (1989).
16. Y. Scribano and C. Leforestier, "Contribution of water dimer absorption to the millimeter and far infrared atmospheric water continuum," J. Chem. Phys. **126**, 234301 (2007).
17. K. Bielska, A. A. Kyuberis, Z. D. Reed, G. Li, A. Cygan, R. Ciurylo, E. M. Adkins, L. Lodi, N. F. Zobov, V. Ebert, D. Lisak, J. T. Hodges, J. Tennyson, and O. L. Polyansky, "Subpromille measurements and calculations of CO (3-0) overtone line intensities," Phys. Rev. Lett. **129**, 043002 (2022).
18. F. Sizov and A. Rogalski, "THz detectors," Prog. Quantum Electron. **34** (5), 278–347 (2010).
19. L. Consolino, S. Bartalini, and P. De Natale, "Terahertz frequency metrology for spectroscopic applications: A review," J. Infrared Millim. Terahertz Waves **38** (11), 1289–1315 (2017).
20. S. Yu, J. C. Pearson, B. J. Drouin, M.-A. Martin-Drumel, O. Pirali, M. Vervloet, L. H. Coudert, H. S. P. Muller, and S. Brunken, "Measurement and analysis of new terahertz and far-infrared spectra of high temperature water," J. Mol. Spectrosc. **279**, 16–25 (2012).
21. L. H. Coudert, G. Wagner, M. Birk, Yu. I. Baranov, W. J. Lafferty, and J.-M. Flaud, "The $H_2{}^{16}O$ molecule: Line position and line intensity analyses up to the second triad," J. Mol. Spectrosc., No. 251, 339–357 (2008).
22. L. H. Coudert, M.-A. Martin-Drumell, and O. Pirali, "Analysis of the high-resolution water spectrum up to

the second triad and to $J = 30$," J. Mol. Spectrosc. **303**, 36–41 (2014).

23. D. W. Schwenke and H. Partridge, "Convergence testing of the analytic representation of an ab initio dipole moment function for water: Improved fitting yields improved intensities," J. Chem. Phys. **113**, 6592 (2000).
24. Z. D. Reed, H. Tran, H. N. Ngo, J.-M. Hartmann, and J. T. Hodges, "Effect of non-markovian collisions on measured integrated line shapes of CO," Phys. Rev. Lett. **130** (143001) (2023).
25. L. Lodi, J. Tennyson, and O. L. Polyansky, "A global, high accuracy ab initio dipole moment surface for the electronic ground state of the water molecule," J. Chem. Phys. **135** (3), 034113 (2011).
26. V. T. Sironneau and J. T. Hodges, "Line shapes, positions and intensities of water transitions near 1.28 μm," J. Quant. Spectrosc. Radiat. Transfer **152**, 1–15 (2015).
27. E. K. Conway, A. A. Kyuberis, O. L. Polyansky, J. Tennyson, and N. F. Zobov, "A highly accurate ab initio dipole moment surface for the ground electronic state of water vapour for spectra extending into the ultraviolet," J. Chem. Phys. **149**, 084307 (2018).
28. S. Vasilchenko, S. N. Mikhailenko, and A. Campargue, "Cavity ring down spectroscopy of water vapor near 750 nm: A test of the HITRAN2020 and W2020 line lists," Mol. Phys. **120** (22051762) (2022).
29. A. M. Solodov, T. M. Petrova, A. A. Solodov, V. M. Deichuli, and O. V. Naumenko, "FT spectroscopy of water vapor in the 0.9 μm transparency window," J. Quant. Spectrosc. Radiat. Transfer **293**, 108389 (2022).
30. T. M. Rubin, M. Sarrazin, N. F. Zobov, J. Tennyson, and O. L. Polyansky, "Sub-percent accuracy for the intensity of a near-infrared water line at 10670 cm^{-1}: Experiment and analysis," Mol. Phys. **120** (19-20), e2063769 (2022).
31. HITRAN database. URL: https://hitran.org/. Cited February 15, 2023.
32. N. Jacquinet-Husson, R. Armante, N. A. Scott, A. Chedin, L. Crepeau, C. Boutammine, A. Bouhdaoui, C. Crevoisier, V. Capelle, C. Boonne, N. Poulet-Crovisier, A. Barbe, Benner D. Chris, V. Boudon, L. R. Brown, J. Buldyreva, A. Campargue, L. H. Coudert, V. M. Devi, M. J. Down, B. J. Drouin, A. Fayt, C. Fittschen, J.-M. Flaud, R. R. Gamache, J. J. Harrison, C. Hill, O. Hodnebrog, S.-M. Hu, D. Jacquemart, A. Jolly, E. Jimenez, N. N. Lavrentieva, A.-W. Liu, L. Lodi, O. M. Lyulin, S. T. Massie, S. Mikhailenko, H. S. P. Muller, O. V. Naumenko, A. Nikitin, C. J. Nielsen, J. Orphal, V. I. Perevalov, A. Perrin, E. Polovtseva, A. Predoi-Cross, M. Rotger, A. A. Ruth, S. S. Yu, K. Sung, S. A. Tashkun, J. Tennyson, Vl. G. Tyuterev, Auwera J. Vander, B. A. Voronin, and A. Makie, "The 2015 edition of the GEISA spectroscopic database," J. Mol. Spectrosc. **327**, 31–72 (2016).
33. GEISA Spectroscopic database. URL: https://geisa.aeris-data.fr/#. Cited February 15, 2023.
34. Jet Propulsion Laboratory, Catalog directory. https://spec.jpl.nasa.gov/ftp/pub/catalog/catdir.html. Cited February 15, 2023.
35. J. Tennyson and S. N. Yurchenko, "ExoMol: Molecular line lists for exoplanet and other atmospheres," Mon. Not. R. Astron. Soc **425** (1), 21–33 (2012).
36. www.exomol.com/. Cited February 15, 2023.
37. T. Furtenbacher, R. Tobias, J. Tennyson, O. L. Polyansky, A. A. Kyuberis, R. I. Ovsyannikov, N. F. Zobov, and A. G. Csaszar, "The W2020 database of validated rovibrational experimental transitions and empirical energy levels of water isotopologues. II. $H_2{}^{17}O$ and $H_2{}^{18}O$ with an update to $H_2{}^{16}O$," J. Phys. Chem. Ref. Data **49**, 043103 (2020).
38. E. K. Conway, I. E. Gordon, A. A. Kyuberis, O. L. Polyansky, J. Tennyson, and N. F. Zobov, "Calculated line lists for $H_2{}^{16}O$ and $H_2{}^{18}O$ with extensive comparisons to theoretical and experimental sources including the HITRAN2016 database," J. Quant. Spectrosc. Radiat. Transfer **241**, 106711 (2020).
39. O. L. Polyansky, A. A. Kyuberis, N. F. Zobov, J. Tennyson, S. N. Yurchenko, and L. Lodi, "ExoMol molecular line lists XXX: A complete high-accuracy line list for water," Mon. Not. R. Astron. Soc. **480** (2), 2597–2608 (2018).
40. R. J. Barber, J. Tennyson, G. J. Harris, and R. N. Tolchenov, "A high-accuracy computed water line list," Mon. Not. R. Astron. Soc. **368**, 1087–1094 (2006).
41. S. V. Shirin, O. L. Polyansky, N. F. Zobov, P. Barletta, and J. Tennyson, "Spectroscopically determined potential energy surface of $H_2{}^{16}O$ up to 25000 cm^{-1}," J. Chem. Phys. **118** (5), 2124–2129 (2003).
42. A. E. Lynas-Gray, S. Miller, and J. Tennyson, "Infrared transition intensities for water: A comparison of ab initio and fitted dipole moment surfaces," J. Mol. Spec. **169**, 458–467 (1995).
43. I. I. Bubukina, N. F. Zobov, O. L. Polyansky, S. V. Shirin, and S. N. Yurchenko, "Optimized semiempirical potential energy surface for $H_2{}^{16}O$ up to 26000 cm^{-1}," Opt. Spectrosc. **110** (2), 160–166 (2011).
44. E. K. Conway, I. E. Gordon, J. Tennyson, O. L. Polyansky, S. N. Yurchenko, and K. Chance, "A semi-empirical potential energy surface and line list for $H_2{}^{16}O$ extending into the near-ultraviolet," Atmos. Chem. Phys. **20**, 10015–10027 (2020).
45. I. I. Mizus, A. A. Kyuberis, N. F. Zobov, V. Yu. Makhnev, O. L. Polyansky, and J. Tennyson, "High-accuracy water potential energy surface for the calculation of infrared spectra," Phil. Trans. R. Soc. Lond. A **376**, 20170149 (2018).
46. G. E. Becker and S. H. Autler, "Water vapor absorption of electromagnetic radiation in the centimeter wavelength range," Phys. Rev. **70** (5-6), 300–307 (1946).
47. H. J. Liebe, M. C. Thompson, and T. A. Dillon, "Dispersion studies of the 22 GHz water vapor line shape: I. The Lorentzian behavior," J. Quant. Spectrosc. Radiat. Transfer **9**, 31–47 (1969).
48. M. Yu. Tretyakov, V. V. Parshin, M. A. Koshelev, V. N. Shanin, S. E. Myasnikova, and A. F. Krupnov, "Studies of 183 GHz water line: Broadening and shifting by air, N_2, and O_2 and integral intensity measurements," J. Mol. Spectrosc. **218**, 239–245 (2003).
49. M. A. Koshelev, M. Yu. Tretyakov, G. Yu. Golubiatnikov, V. V. Parshin, V. N. Markov, and I. A. Koval, "Broadening and shifting of the 321-, 325-, and 380-GHz lines of water vapor by the pressure of atmospheric gases," J. Mol. Spectrosc. **241**, 101–108 (2007).